Transgenic mouse models in migraine

Ven, R.C.G. van de

Chapter 2B

Morphological assessment in the transgenic R192Q *Cacna1a* knockin migraine mouse model by *in vivo* high-resolution MRI

R.C.G. van de Ven,[1] R. van der Landen,[2] L. van der Weerd,[3] M. Fodor,[3] J.H.C. Reiber,[2] R.E. Poelmann,[3] M.A. van Buchem,[2] M.D. Ferrari,[4] R.R. Frants,[1] A.M.J.M. van den Maagdenberg,[1,4] F. Admiraal-Behloul[2]

Department of [1]Human Genetics, [2]Radiology, [3]Anatomy & Embryology and [4]Neurology, Leiden University Medical Centre, Leiden, The Netherlands

Based on:

Proceedings of the 3rd IEEE-ISBI, 406-409, 2006

Proceedings of the 14th Intl. Soc. Magn. Reson. Med., 3391, 2006

Abstract

Because of its close genetic and physiological similarities to humans, as well as the ease with which its genome can be manipulated, the mouse became the mammalian model of choice for genetic research. A first step in describing the potential impact of a given genetic manipulation is the characterization of general morphology. The use of 3–dimensional imaging techniques with high spatial resolution, such as magnetic resonance imaging (MRI), became crucial because such imaging tools can expedite anatomical phenotyping in the genetically altered mice. In this paper we describe a semi-automatic MRI image brain segmentation and its application to phenotypical characterization of brain structures in a migraine mouse model, assessing volume and morphology of the cerebellar white matter and the brain ventricles. Our segmentation is atlas-based and is designed for *in vivo* MRI image analysis.

Introduction

Over the past century, the mouse has developed into the premier mammalian model system for functional genetic research. This is mainly because of its close genetic and physiological similarities to humans, as well as the relative ease with which its genome can be manipulated and analyzed.

Mice are the tools of choice for probing the immune, endocrine, nervous, cardiovascular, skeletal and other complex physiological systems that mammals share. The major goal of biological studies is to understand and characterize the effects of genotype on anatomy, physiology, behavior, and ultimately the role of genotype in development of disease. The use of imaging techniques with high spatial resolution potential is rising because such imaging tools can expedite anatomical phenotyping in the genetically altered mice. Anatomical phenotyping is the first step in describing the potential impact of a given genetic manipulation and begins with the characterization of general morphology.

Magnetic resonance imaging (MRI) is a noninvasive, inherently three-dimensional (3D) imaging technique capable of visualizing several anatomical structures in the mouse. The 3D nature of MRI also allows for interpretation of complex spatial relationships between substructures, which is important when phenotyping anatomically.

Migraine is a neurological paroxysmal disorder affecting up to 16% in the general population Patients suffer from throbbing, often unilateral headaches lasting 4 to 72 hours that are accompanied by nausea, vomiting and/or photo- and phonophobia. Familial hemiplegic migraine type-1 (FHM1) is an autosomal dominant subtype of migraine with aura caused by mutations in the *CACNA1A* gene. This gene encodes the pore forming

α_1-subunit of $Ca_v2.1$ (P/Q-type) calcium channels.

Recently, a transgenic knockin (KI) mouse model of migraine has been generated by our group that contains a human pathogenic R192Q FHM1 mutation in the orthologous mouse *Cacna1a* gene.[1] In patients, the R192Q mutation is associated with FHM1 without additional clinical features.[2] It was shown that R192Q KI mice have increased Ca^{2+} influx through mutated $Ca_v2.1$ channels, enhanced neurotransmitter release and an increased susceptibility to cortical spreading depression (CSD, the likely mechanism for the migraine aura).[1]

Particularly in migraine with aura patients with high attack frequency, sub-clinical white matter abnormalities were found in regions of the cerebellum and brainstem.[3,4] In addition, morphological abnormalities have been found in various headache syndromes.[5,6,7] The nature of these MRI abnormalities is not known.

The purpose of this work was to use MRI for *in vivo* phenotypical characterization of brain structures in migraine mouse models. A precursor to the analysis of brain structures in MRI images is their segmentation. Although considerable progress has been made in automated human brain segmentation, the mouse has received very little attention. Most of the published studies that required volume analysis of structures have used manual tracings, which are tedious and error prone.

Recent automatic segmentation methods were designed for *ex vivo* brain images and require a very good image contrast (Fig. 1A).[8] *In vivo* images, however, present much less contrast in most sub-cortical structures (Fig. 1C) and therefore are more challenging for automatic image segmentation. Furthermore, a brain-stripping step is required as the image displays the brain within the skull of the mouse.

We hypothesized that if lesions would be present in R192Q KI mice, lesion load increases with age. Therefore, in this paper we image aged R192Q KI mice *in vivo* and describe a simple automatic approach for segmentation of the cerebellum and brain ventricles in MRI images of mouse brain. We present the results of its successful application to MRI images for a comparative analysis of the volumes and morphology in R192Q KI migraine mice and littermates.

Material and Methods

Mice

In vivo imaging was performed on 11 homozygous R192Q KI mice[1] and 11 wild-type (WT) littermates. All mice were aged 19.9 ± 3.3 months. For MRI, mice were initially anaesthetized with 4% isoflurane in air (50%) and O_2 (50%) and maintained with ~1.5% isoflurane during the procedure. The respiratory rate was monitored via an air-pressure cushion connected to a laptop using Biotrig software (Bruker, Rheinstetten, Germany).

Magnetic Resonance Imaging

Imaging was performed on a 9.4 T vertical 89-mm-bore magnets (Bruker BioSpin, Rheinstetten, Germany) with a Bruker Micro2.5 gradient system of 1 T/m and a transmit/receive birdcage radio frequency coil with an inner diameter of 30 mm. Bruker ParaVision 3.0 software was used for image acquisition. Anatomical images were acquired using a T_2-weighted multi-slice spin echo sequence. Imaging parameters were: TE = 35 ms, TR = 6 s, FOV = 25.6 mm, matrix = 256×256, 40 slices of 0.2 mm thickness, 4 averages.

Automatic image segmentation and volume calculation

Our segmentation approach is template based and is very similar to our work on the automatic segmentation of the human brain.[9] An average *in vivo* T_2-weighted brain image has been generated from 6 randomly selected images that were manually aligned to the SHIVA *ex vivo* brain template (Synchronized Histological Image Visualization Architecture, UCLA, Los Angelos, CA)[10] using 9-parameter linear transformation (Fig. 1A,D). We used the SHIVA masks to visually control and guide the manual registration. As showed in figure 1a, the brain ventricle mask of the SHIVA template is quite thin; this is mainly because this template was generated on images of a younger mouse (3 months old). Furthermore, being an *ex vivo* brain, the ventricular cavity might have lost its original size and shape. Therefore, we manually defined a coarse ventricular area on the template image which would be large enough to include ventricles of different sizes (Fig. 1E). The carefully aligned average T_2-weighted image (Fig. 1B), the SHIVA masks, and our ventricular region where considered, all together (Fig. 1E), as the *in vivo* brain atlas for our semi-automatic segmentation.

The automatic segmentation consisted of four main steps:

1. Template mapping

The average T_2-weighted image has been automatically registered to every mouse image

using a 12-parameter affine transformation. Using the transformation matrix resulting from the automatic registration, we mapped the masks of the intracranial cavity, the cerebellum and the manually defined brain ventricle area (Fig. 1E) on every image.

2. Brain ventricle segmentation

In a T_2-weighted MR image, the cerebrospinal fluid is hyperintense. Using a fuzzy clustering algorithm (FCM)[11], we clustered the brain voxels (yellow mask in Fig. 1) in to 3 clusters: dark, medium-dark and bright. All voxels with a signal intensity higher than the bright-cluster prototype and falling in the vicinity of the manually defined ventricular area, were classified as ventricular voxels (Fig. 1F).

*3. Cerebellar white matter segmentatio*n

In a T_2-weighted MR image at 9.4 T, the white matter is hypointense. Using the FCM algorithm, we clustered all the signal intensities of the voxels within the template mask of cerebellum, into 2 clusters: dark and bright. All the voxels with signal intensity lower than the prototype of the dark-cluster were classified as cerebellar white matter (Fig. 1F).

4. Manual verification and correction of segmentation

Results from the automatic segmentation were manually verified and corrected.

After the semi-automatic segmentation of whole brain, total ventricles, fourth ventricle and cerebellum, volume measurements of each structure were performed by multiplying voxel-count with voxel size. Volumes were normalized to whole brain volume.

Evaluation method for the automatic segmentation

For the evaluation and validation of the automatic segmentation of *in vivo* data, we considered manual delineation as the gold standard. We generated expert manual-delineation of the brain ventricles and the cerebellum in 9 mice. Manual delineation of the white matter was not carried out. In order to evaluate the spatial agreement between the gold standard and the automatic segmentation we used the similarity index defined as follow:

$$SI(GS, Auto) = \frac{2 * (GS \cap Auto)}{GS + Auto}$$

where GS is used for gold standard and Auto for the fully automatic segmentation.

$GS \cap Auto$ refers to the volume of the overlap between Auto and GS. The SI takes values between 0 and 1; 0 for no overlap at all (total disagreement) and 1 for a perfect alignment of the two (ideal). An SI value of 0.7 or higher indicates a very good to excellent agreement.[12]

Group comparison

In order to analyze the morphometry of the segmented brain structures, the images must first be normalized in order to correct for head size, position and orientation. We aligned, all the images to the SHIVA space by automatic registration to our *in vivo* template using 12-parameter affined transformations. The average MR image of controls and of R192Q KI migraine mice was then generated.

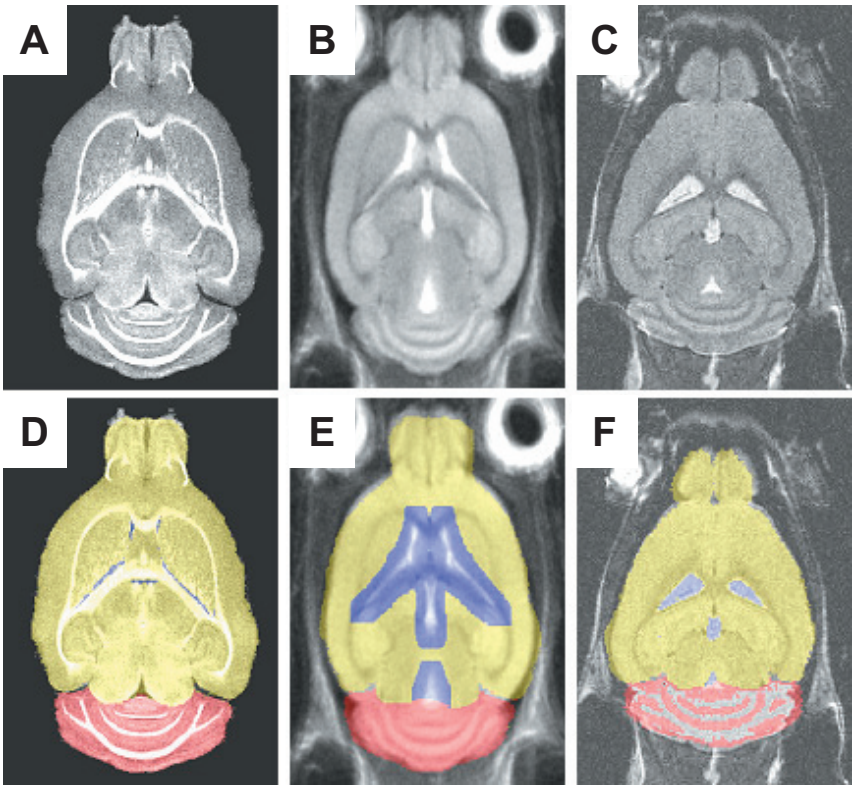

Figure 1. (**A**) the SHIVA *ex vivo* brain (**B**), *in vivo* average brain and (**C**) *in vivo* single mouse brain image. (**D**) the SHIVA template with masks, (**E**) *in vivo* average brain template and (**F**) outcome of automatic segmentation of an individual mouse brain. Masks of whole brain (yellow), ventricles (blue) and cerebellum (red) are shown.

A free-form deformation image registration method[13] was used to co-register the average wild-type image (moving image) on the average R192Q KI image (fixed image). The output of the registration is a non-linear deformation field that gives for each voxel

of the moving image a displacement vector toward the matched voxel in the fixed image. From each displacement vector, the orientation and the amplitude can be derived.

Results

Automatic segmentation validation

On the outcome of the segmentation of the brain ventricles, we obtained an average SI value of 0.83 with 95% confidence interval of [0.76, 091] and a standard deviation (SD) of 0.04. For the cerebellum, we considered the SHIVA masks after mapping without any further processing. We obtained a SI of 0.79 with 95% confidence interval of [0.73, 0.81] and a SD of 0.02. These values indicate an excellent agreement with expert manual delineation. The white matter segmentation has been evaluated visually on every slice for every mouse. The results were very satisfactory (figure 1F).

Table 1 Volumetric results and *p*-values

	Wild-type	R192Q KI	*p*-value
Absolute Volumes			
Total brain volume	469.4 ± 12.2	466.7 ± 18.3	0.696
Normalized			
Cerebellum	10.84 ± 0.28	11.12 ± 0.29	0.030†
Ventricles	1.73 ± 0.24	1.76 ± 0.21	0.694
4th Ventricle	0.38 ± 0.07	0.34 ± 0.05	0.130

Absolute volumes in µl ± SD. Normalized values in % of total brain volume ± SD. Two-tailed Student's t-test. †$p < 0.05$.

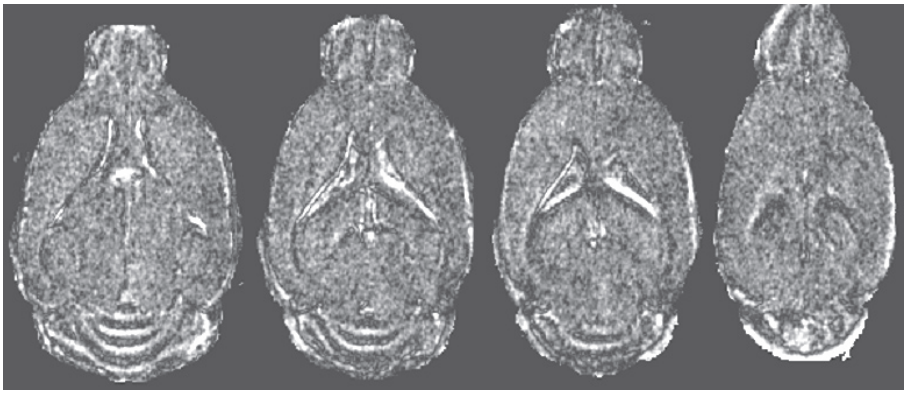

Figure 2. Absolute difference images between the average R192Q KI migraine mouse T_2-weighted brain image and the average control brain. Slices at different brain levels are shown. Note that the highest differences are mainly at the areas of the ventricles and cerebellum.

Volumetric analysis

Table 1 shows volumetric measurements of whole brain. Whole brain volume was not different between wild-type and R192Q KI mice. Volumes of total ventricles, fourth ventricle and cerebellum were normalized to whole brain volume. Cerebellar volume was slightly increased with respect to whole brain volume (p=0.030), while total ventricle and fourth ventricle volumes remained unchanged.

Morphometry

In addition to increased volume, we found a difference in shape of the cerebellum between the two groups. Figure 2 shows a difference image (absolute values) of the

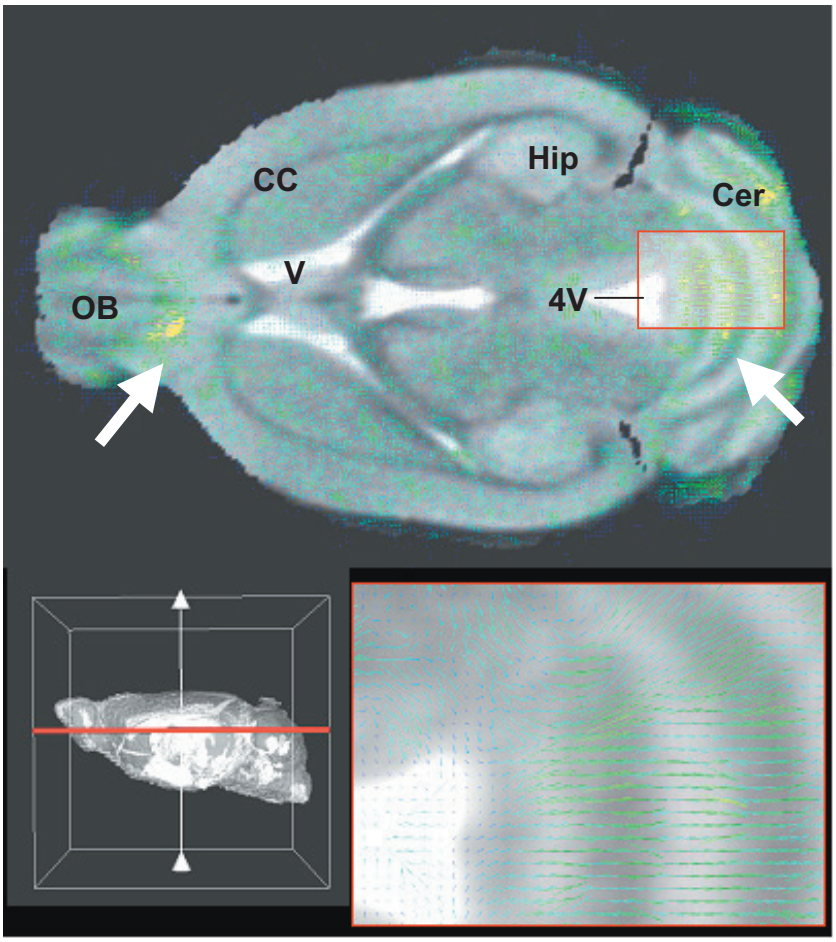

Figure 3. Deformation field analysis showing deformation (green) mainly at the olfactory bulb and cerebellum (white arrows). The inset shows a caudal shift of the cerebellum. 4V, fourth ventricle; CC, corpus callosum; Cer, cerebellum; Hip, hippocampus; OB, olfactory bulb; V, ventricle

average migraine mouse and the average control mouse: the larger the image intensity, the larger the image difference. One can note that most of the differences were found in the cerebellum and the ventricle areas, while structures like the corpus callosum and the hippocampus did not show any noticeable difference. To study these differences in more detail, we performed deformation field analysis, which shows the extent and direction of changes between groups, confirming that the largest differences between R192Q KI mice were at the olfactory bulb and the cerebellum (Fig. 3). Vector field analysis indicates cerebellar displacement in caudal direction.

Discussion

In this paper we presented a preliminary study on brain morphology of old R192Q KI mice using a simple semi-automatic segmentation technique. The outcome of the segmentation was quantitatively compared to expert delineation of 9 mice MRI images. The similarity indices in all 9 mice were higher than 0.74. Thus, semi-automatic segmentation was in excellent agreement with expert delineation, validating the technique.

The segmentation was successfully applied in order to morphologically characterize the cerebellum and ventricular structures in R192Q KI migraine mice. Our main finding was an increase in cerebellar volume, together with a displacement of the cerebellum in R192Q KI mice, a brain region in which $Ca_v2.1$ channels are highly expressed.[14] Cerebellar displacement is probably neither due to in- or decreased fourth ventricle volume (Table 1, Fig. 3). Preliminary results from histological analysis indicate that these changes are not associated with obvious pathology detectable in fixed tissue, neither in the cerebellum nor in any other brain region.

R192Q KI mouse do not have obvious behavioral abnormalities that would indicate pathological cerebellar dysfunction.[1] However, there are indications of subclinical cerebellar involvement in migraine.[15] Moreover, particularly in migraine with aura patients with high attack frequency, sub-clinical white matter abnormalities were found mainly in regions of the cerebellum and brainstem.[3,4] This indicates that the migraine aura may be an import factor in the pathogenesis of these lesions. Neuroimaging findings indicate that the migraine aura is due to cortical spreading depression (CSD), a wave of transient intense spike activity that progresses slowly along the cortex and is followed by a long-lasting neuronal suppression.[16-19] Earlier results showed that the transgenic R192Q FHM1 mice exhibited an increased susceptibility to CSD.[1] CSD is known to induce blood-brain barrier disruption and leads to edema in a rat model.[20] Therefore, cerebellar volume increase and caudal displacement may be caused by edema, which is not visible on histological sections due to tissue fixation and dehydration that preceded

paraffin embedding.

In conclusion, we analyzed *in vivo* brain morphology of old R192Q KI mice using MRI combined with a simple automatic segmentation technique for volume measurements. A slight increase in cerebellar volume and a caudal displacement were found.

References

1. Van den Maagdenberg,A.M. *et al.* A cacna1a knockin migraine mouse model with increased susceptibility to cortical spreading depression. *Neuron* **41**, 701-710 (2004).
2. Ophoff,R.A. *et al.* Familial hemiplegic migraine and episodic ataxia type-2 are caused by mutations in the Ca2+ channel gene CACNL1A4. *Cell* **87**, 543-552 (1996).
3. Kruit,M.C. *et al.* Migraine as a risk factor for subclinical brain lesions. *JAMA* **291**, 427-434 (2004).
4. Kruit,M.C., Launer,L.J., Ferrari,M.D. & van Buchem,M.A. Brain stem and cerebellar hyperintense lesions in migraine. *Stroke* **37**, 1109-12 (2006).
5. May,A. *et al.* Correlation between structural and functional changes in brain in an idiopathic headache syndrome. Nat Med. 1999 Jul;5(7):836-8.
6. Rocca,M.A. *et al.* Brain gray matter changes in migraine patients with T2-visible lesions: a 3-T MRI study. *Stroke* **37**, 1765-70 (2006).
7. Schmidt-Wilcke,T. *et al.* Gray matter decrease in patients with chronic tension type headache.*Neurology* **65**, 1483-6 (2005).
8. Ali,A.A., Dale,A.M., Badea,A. & Johnson,G.A. Automated segmentation of neuroanatomical structures in multispectral MR microscopy of the mouse brain. *Neuroimage.* **27**, 425-435 (2005).
9. Admiraal-Behloul,F. *et al.* Fully automatic segmentation of white matter hyperintensities in MR images of the elderly. *Neuroimage.* **28**, 607-617 (2005).
10. http://www.loni.ucla.edu/MAP/Atlas/MAP_Software.html
11. Dave,R. & Krishnapuram,R. Robust clustering methods: a unified view. *IEEE Trans. Fuzzy Systems* **5**, 270-293 (1997).
12. Bartko,J.J. Measurement and reliability: statistical thinking considerations. *Schizophr. Bull.* **17**, 483-489 (1991).
13. Thirion,J.P. Image matching as a diffusion process: an analogy with Maxwell's demons. *Med Image Anal.* **2**, 243-260 (1998).
14. Westenbroek,R.E. *et al.* Immunochemical identification and subcellular distribution of the alpha 1A subunits of brain calcium channels. *J. Neurosci.* **15**, 6403-6418 (1995).
15. Sandor,P.S. *et al.* Subclinical cerebellar impairment in the common types of migraine: a three-dimensional analysis of reaching movements. *Ann Neurol* **49**, 668-72 (2001).
16. Bowyer,S.M., Aurora,K.S., Moran,J.E., Tepley,N. & Welch,K.M. Magnetoencephalographic fields from patients with spontaneous and induced migraine aura. *Ann. Neurol.* **50**, 582-587 (2001).
17. Cutrer,F.M., O'Donnell,A. & Sanchez,d.R. Functional neuroimaging: enhanced understanding of migraine pathophysiology. *Neurology* **55**, S36-S45 (2000).
18. Hadjikhani,N. *et al.* Mechanisms of migraine aura revealed by functional MRI in human visual cortex. *Proc. Natl. Acad. Sci. U. S. A* **98**, 4687-4692 (2001).
19. Lauritzen,M. Pathophysiology of the migraine aura. The spreading depression theory. *Brain* **117**, 199-210 (1994).
20. Gursoy-Ozdemir,Y. *et al.* Cortical spreading depression activates and upregulates MMP-9. *J. Clin. Invest* **113**, 1447-1455 (2004).